Spatial quantitative metabolomics enables identification of remote and sustained ipsilateral cortical metabolic reprogramming after stroke

Wang, G.Q.; Berg, B.M. van den; Kostidis, S.; Pinkham, K.; Jacobs, M.E.; Liesz, A.; ... ; Rabelink, T.J.

Citation

Wang, G. Q., Berg, B. M. van den, Kostidis, S., Pinkham, K., Jacobs, M. E., Liesz, A., … Rabelink, T. J. (2025). Spatial quantitative metabolomics enables identification of remote and sustained ipsilateral cortical metabolic reprogramming after stroke. *Nature Metabolism*, *7*(9), 1791-1800. doi:10.1038/s42255-025-01340-8

nature metabolism

Letter

https://doi.org/10.1038/s42255-025-01340-8

Spatial quantitative metabolomics enables identification of remote and sustained ipsilateral cortical metabolic reprogramming after stroke

Received: 4 October 2024

Accepted: 23 June 2025

Gangqi Wang[1,2] ✉, Bernard M. van den Berg[2,3], Sarantos Kostidis[4], Kelsey Pinkham[5,6], Marleen E. Jacobs[2,3], Arthur Liesz[5,6], Martin Giera[3,4] ✉ & Ton J. Rabelink[2,3] ✉

Mass spectrometry imaging (MSI) has become a cornerstone of spatial biology research. However, various factors that are intrinsic to the technology limit the quantitative capacity of MSI-based spatial metabolomics and thus reliable interpretation. Here we developed an improved quantitative MSI workflow, based on isotopically ^{13}C-labelled yeast extract as internal standards, to overcome these pitfalls. Using brain and kidney tissue, we demonstrate that this approach allows for quantification of more than 200 metabolic features. Applying our workflow to a stroke model allowed us to not only map metabolic remodelling of the infarct and peri-infarct area over time, but also discover hitherto unnoted remote metabolic remodelling in the histologically unaffected ipsilateral sensorimotor cortex. At day 7 post-stroke, increased levels of neuroprotective lysine and reduced excitatory glutamate levels were found when compared with the contralateral cortex. By day 28 post-stroke, lysine and glutamate levels appeared normal, while decreased precursor pools of uridine diphosphate *N*-acetylglucosamine and linoleate persisted that were previously linked to vulnerability. Importantly, traditional normalization strategies not using internal standards were unable to visualize these differences. Using ^{13}C-labelled yeast extracts as a normalization strategy establishes a paradigm in quantitative MSI-based spatial metabolomics that greatly enhances reliability and interpretive strength.

Spatial biology has taken centre stage in life science and biotechnology research. Spatially resolved molecular technologies are now allowing researchers to shed light on the spatial heterogeneity of biological tissues, micro-environments and cell–cell communications, integrating biology's central disciplines: transcriptome, epigenome, proteome and metabolome[1]. Spatial metabolomics, as an important component of spatial biology, provides insights into the in situ distribution of metabolites and metabolic micro-environments. MSI-based spatial metabolomics serves as the primary approach for examining the spatial distribution of metabolites[2]. However, several pitfalls (for example, matrix effect, adduct formation and in-source fragmentation) render MSI-based quantification cumbersome if not impossible[3,4]. These challenges are intrinsic to mass spectrometry (MS) based approaches and consequently affect both major MSI technologies, matrix-assisted laser desorption ionization (MALDI) and desorption electrospray ionization (DESI)[5,6]. Even more so, these limitations can affect both

---

A full list of affiliations appears at the end of the paper. ✉e-mail: g.wang@lumc.nl; m.a.giera@lumc.nl; a.j.rabelink@lumc.nl

intertissue comparison and, more critically, regional comparisons in a single tissue[5]. Batch effects caused by day-to-day experimental and instrumental variations further complicate the matter[7]. In summary, the quantification and standardization of spatial metabolomics is jeopardized by various analytical intricacies that have yet to be overcome. The most widely accepted and practised approach for enabling (absolute) quantification and reducing intra- and interbatch variations is the use of isotopically labelled internal standards (IS), commonly using ^{13}C-labelled variants[3]. Such a strategy has recently been applied to spatial lipidomics analysis, compensating for the matrix effect and ensuring data reproducibility across different laboratories[8]. This method involves the use of class-specific IS homogeneously applied to the tissue surface. The approach is facilitated by the fact that lipids follow a building block structure with lipid class chemical properties largely being dictated by the lipid headgroup[9]. Consequently, a limited number of only 13 class-specific IS could serve as reference points for pixelwise normalization of each lipid species in the tissue sample. However, extrapolating the concept to spatial metabolomics studies presents challenges because of the more-diverse physico-chemical properties of (water-soluble) metabolites compared with lipids. Even for distinct metabolite classes, physico-chemical properties and structures can differ vastly, necessitating metabolite-specific rather than class-specific IS. However, use of extended metabolite IS panels can be costly or constrained by availability, particularly when working at omics-scale. Alternatively, uniformly ^{13}C-labelled (U-^{13}C) yeast extracts offer a rich source of isotopically labelled metabolites derived from evolutionarily conserved primary metabolomes. These extracts have been used as IS for quantitative metabolomics with liquid chromatography–mass spectrometry (LC–MS) and gas chromatography–mass spectrometry[10,11]. Relying on the biosynthetic machinery of yeast to generate a multitude of ^{13}C-labelled metabolite standards, we here introduce a quantitative spatial metabolomics method that combines ^{13}C-labelled yeast extracts with MALDI-MSI, enabling pixelwise IS normalization or relative quantification of more than 200 metabolic features.

This quantitative MSI method is based on previously validated 'on-tissue' spraying approaches[12]. U-^{13}C-labelled yeast extracts were homogeneously sprayed onto a heat-inactivated tissue surface, followed by deposition of *N*-(1-naphthyl) ethylenediamine dihydrochloride (NEDC) matrix, as described previously[13]. Detection of in situ metabolic features in negative mode was performed using a TimsTOF flex MALDI2 mass spectrometer (Fig. 1a). Tissues sprayed with and without ^{13}C-labelled yeast extracts exhibited comparable spectrum quality, enabling the putative identification of yeast-derived ^{13}C-labelled metabolites (Extended Data Fig. 1). To investigate the overall matrix effect of metabolites, we performed molecular histology, as we described previously using colour code generated from three- dimensional uniform manifold approximation and projection (UMAP) analysis[13], based on both yeast-derived ^{13}C-labelled metabolites and endogenous lipids to visualize tissue structure in kidney and brain (Fig. 1b). The exogenous metabolites exhibited histological signals similar to tissue structures (Fig. 1b), whereas various sprayed ^{13}C-labelled metabolites showed a distinct matrix effect in each tissue sample (Extended Data Fig. 2a,b). These findings underscore the importance of correcting matrix effect for individual metabolites in spatial metabolomics studies. Overall, we detected 427 metabolite or lipid features present in both unlabelled and ^{13}C-labelled yeast extracts, jointly serving as potential IS for subsequent normalization and quantification (Fig. 1c and Supplementary Table 1). We examined the presence of both endogenous unlabelled metabolic features and their corresponding exogenous ^{13}C-labelled metabolites in kidney and brain tissues sprayed with ^{13}C-labelled yeast extracts, excluding overlapping peaks. Overall, 171 and 170 metabolite or lipid features were found useful for pixelwise normalization on kidney and brain respectively, and 145 features could be applied to both tissues (Fig. 1c and Supplementary Table 2). These metabolic features are biochemically involved in glycolysis–gluconeogenesis, the tricarboxylic acid (TCA) cycle, pentose phosphate pathway, and amino acid and fatty acid metabolic pathways (Fig. 1d). Specific examples include glutathione (GSH), glutathione disulfide (GSSG), uridine diphosphate *N*-acetylglucosamine (UDP-GlcNAc) and reduced nicotinamide adenine dinucleotide. In addition, the identified labelled IS also included more-complex lipids, which can serve to normalize individual lipid species (and classes). Subsequently we selected several lipid IS for class-wise normalization allowing the quantification of more than 100 lipid features belonging to the following lipid classes lysophosphatidic acid, lysophosphatidylethanolamine (LPE), lysophosphatidylinositol, phosphatidylethanolamine (PE), phosphatidic acid (PA), bis(monoacylglycero)phosphate (BMP) or phosphatidylglycerol (PG), phosphatidylinositol and phosphatidylserine (PS) (Supplementary Table 3). Ultimately, 146 lipid features from 8 lipid classes could be quantified on brain tissues in addition to 131 metabolic features (Supplementary Table 4). To assess the variability of sprayed IS on tissue, we compared the standard deviation of ^{13}C-labelled metabolites with that of endogenous metabolic features in a homogeneous region (cluster 16 in Fig. 2a). The ^{13}C-labelled group exhibited lower standard deviation but higher relative standard deviation, primarily owing to differences in mean peak intensity (Extended Data Fig. 2c–f). When comparing metabolic features with similar intensities below 100, which covers the majority of sprayed IS and endogenous metabolites, both standard deviation and relative standard deviation were comparable between ^{13}C-labelled and endogenous metabolic features (Extended Data Fig. 2g,h). These results suggest homogeneous spraying of IS on tissue. To test IS correction performance, we subsequently compared relative quantification with the commonly applied root mean square (RMS) and total ion count (TIC) normalization methods. While both traditional normalization methods demonstrated enhancements compared with no normalization, they presented with vastly different results when compared with individual ^{13}C-labelled IS (Fig. 1e,f).

Consequently, to demonstrate the potential of this quantitative method for biological discovery, we conducted region-specific analysis on mouse brains in an experimental photothrombotic stroke model[14]. Samples from both day 7 post-stroke (subacute phase) and day 28 post-stroke (chronic phase) were analysed. Integrating haematoxylin and eosin staining on post-MSI tissue with spatial segmentation of the MALDI-MSI data, UMAP of lipid features revealed five distinct infarct (clusters 12, 21 and 26) and peri-infarct (clusters 20 and 25) regions (Fig. 2a,b and Extended Data Fig. 3). Between the infarct core and peri-infarct areas at day 7, an intermediate region was characterized by a higher presence of BMP or PG 44:12 (Fig. 2c). LC–MS data revealed that it is potentially a mixture of PG 44:12 and BMP 44:12 (Supplementary Table 4). Given the importance of BMP lipids for lysosomal function and the biochemical involvement of PG lipids in their biosynthesis, we postulate that these lipid changes indicate phagocytosis of cellular debris and lysosomal activity[15,16]. At day 28, PS 38:4 was increased, especially in the peri-infarct area (Fig. 2d). PS 38:4 has been identified as a marker of in-stent restenosis in patients[17], which suggests a potential sustained vascular abnormality at day 28. In addition to changes in lipid feature distribution, more than 60% of the 131 detected metabolic features exhibited significant differences across regions (Fig. 2e), highlighting an impact on cellular metabolism following stroke. For example, a gradual decrease in the GSSG/GSH ratio was observed from the necrotic core to peri-infarct regions (Fig. 2f), indicating increased oxidative stress levels as a result of the insult. At day 28 post-stroke, the infarct region showed a higher GSSG/GSH ratio and higher linoleate levels compared with the peri-infarct region, although the GSSG/GSH ratio was still below day 7 levels (Fig. 2f,g). Linoleate could potentially further participate in regulating neurotransmission through its oxidized derivatives upon ischaemic brain stroke[18].

Interestingly, in the absence of any histological changes we observed remote metabolic remodelling in the ipsilateral sensorimotor

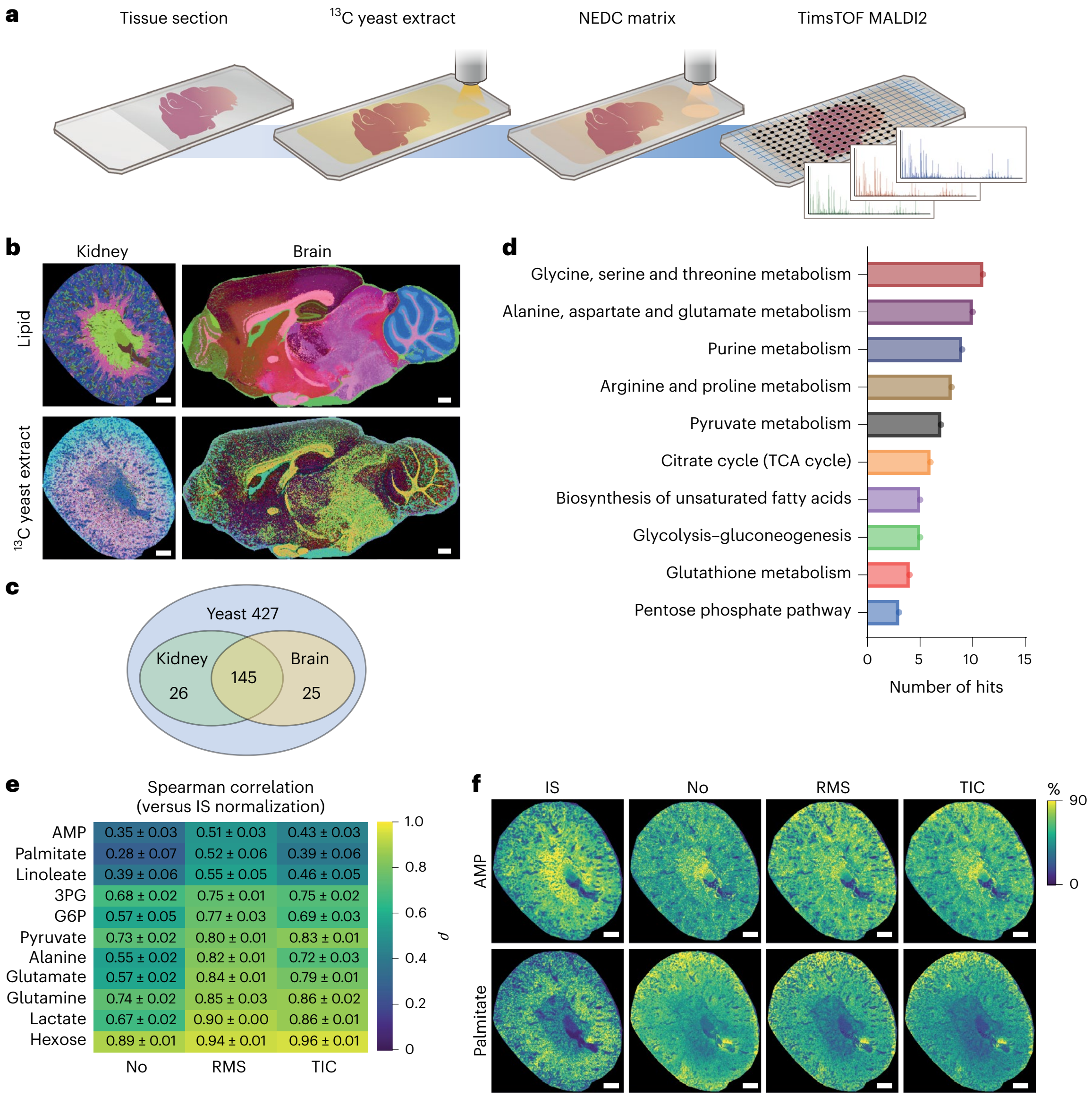

Fig. 1 | ^{13}C yeast-assisted MSI for relative quantitative spatial metabolomics. **a**, Workflow of quantitative spatial metabolomics. **b**, Comparison of molecular histology generated from endogenous lipids only and from exogenous ^{13}C-labelled metabolites and lipids from yeast extract. **c**, Number of available IS from yeast extract and its availability on kidney and brain segments. **d**, Kyoto Encyclopedia of Genes and Genomes pathway analysis on the quantitative metabolic features of both kidney and brain. **e**, Spearman correlation analysis between IS normalization with RMS, TIC or no normalization methods from kidney data ($n = 3$). **f**, Distribution of adenosine monophosphate (AMP) and palmitate using different normalization methods. G6P, glucose-6-phosphate; 3PG, 3-phosphoglyceric acid. Colour bar indicates ratio of peak intensity of each pixel to the maximal intensity of the measured tissue. Scale bars, 600 µm.

cortex region (cluster 16) of the stroke area, in comparison with the contralateral cortical region (cluster 6) (Figs. 2a,b and 3a). To assess potential structural damage in the cortical regions after stroke, myelination was assessed using myelin basic protein (MBP) as an established marker of axonal myelination (Fig. 3b). This ipsilateral cortical region showed normal myelin coverage and cell number compared with its contralateral cortical region (Fig. 3b), indicating an absence of structural brain damage. Based on morphology we could compare cluster 16 with its contralateral region located in the non-affected brain hemisphere in cluster 6 (Fig. 3a). 23 of 131 quantified metabolic features and 61 of 146 quantified lipid features were significantly changed at day 7 post-stroke, and 37 metabolic features and 59 lipid features were significantly changed at day 28 post-stroke (Fig. 3c). This distinct metabolic remodelling in the cluster 16 region at days 7 and 28 post-stroke showed different phases of metabolic remodelling (Fig. 3c). Two distinct *m/z* values (436.283 and 464.314) abundantly present in cluster 16 over time (Fig. 3d,e) were preliminarily or putatively annotated (pre-annotated) as LPE O-16:1 and LPE O-18:1 using database search and off-tissue liquid chromatography–tandem mass spectrometry (LC–MS–MS) analysis as described below. LPE have been implicated in stimulating neurite outgrowth in cultured cortical neurons[19], suggesting a potential contribution to stroke recovery in the cluster 16 region. Decreased glutamate and increased lysine levels were observed in cluster 16 at day 7 post-stroke, which were normalized at 28 days post-stroke compared with control cluster 6 (Fig. 3f,g). Glutamate has been shown to increase the affinity of acid-sensing ion channels for protons and is associated with aggravation of ischaemic neurotoxicity[20], while lysine could inhibit glutamate-induced neuronal activity and is associated with a reduction in the effects of cerebral ischaemic insults[21]. These data suggest protective metabolic remodelling in the ipsilateral

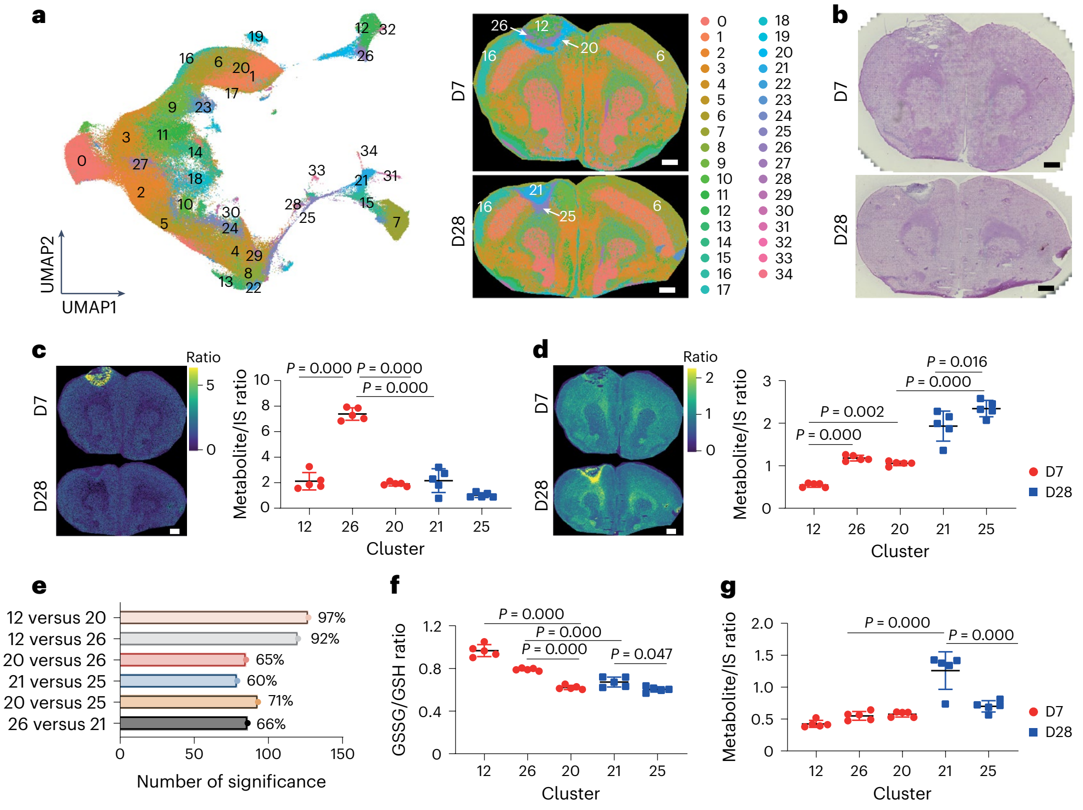

Fig. 2 | Metabolic remodelling after ischaemic stroke revealed by quantitative spatial metabolomics. a, Brain regional segmentation based on MSI-derived lipid profiles of day 7 post-stroke (D7) and day 28 post-stroke (D28) samples ($n = 5$ per group). Left: UMAP results based on MSI-derived lipid profiles. Right: distribution of clusters from the UMAP analysis. Numbers indicate clusters from UMAP analysis. **b**, Representative haematoxylin and eosin staining of post-MSI tissue ($n = 5$ per group). **c**, Left: representative image showing BMP or PG 44:12 distribution in the post-stroke brains ($n = 5$ per group). Right: relative quantification of BMP or PG 44:12 in infarct (clusters 12, 26 and 21) and peri-infarct (clusters 20 and 25) areas. One-way ANOVA followed by Tukey's HSD test were performed. **d**, Left: representative image showing PS 38:4 distribution in the post-stroke brains ($n = 5$ per group). Right: relative quantification of PS 38:4 in infarct and peri-infarct areas. One-way ANOVA followed by Tukey's HSD test were performed. Colour bars in (**c**,**d**) indicate ratio of metabolite to internal standard. **e**, Graph showing the number of significantly changed metabolic features between different areas and its percentage over 131 metabolic features. **f**, GSSG/GSH ratio in infarct and peri-infarct areas ($n = 5$ per group). One-way ANOVA followed by Tukey's HSD test were performed. **g**, Relative quantification of linoleate in infarct and peri-infarct areas ($n = 5$ per group). One-way ANOVA followed by Tukey's HSD test were performed. All data in the plots are presented as mean ± s.d. Scale bars, 600 µm.

cortical region after hypoxic injury in the subacute phase of stroke. At day 28 post-stroke, however, the *O*-GlcNAcylation precursor pools of UDP-GlcNAc and linoleate were significantly reduced (Fig. 3h–i), suggesting long-term sustained metabolic rewiring in the remote ipsilateral cortical region after stroke. UDP-GlcNAc availability is directly associated with *O*-GlcNAcylation of neuronal proteins and protection of ischaemic injury[22]. Similarly, linoleate availability has been related to potential lower stroke risk[23]. Such longer term metabolic remodelling could render the brain vulnerable to further injury.

To validate our ^{13}C-labelled IS based methodology, we also compared these results with the traditional RMS and TIC normalization methods. Comparing the average peak intensities of four metabolites of interest in cluster 16 with its contralateral region revealed various outcomes, of which none was consistent with the IS normalization method (Fig. 3f–j and Extended Data Fig. 4a–c), although matrix effects are generally recognized as region specific. This phenomenon indicates that alteration of analyte composition upon injury will affect the matrix effect of MSI measurements even when comparing similar regions. To prove this, we further compared the peak intensities of all 170 homogenously deposited IS between cluster 16 and its contralateral region using different normalization methods. A significant number of IS resulted in altered peak intensity between contralateral regions (Fig. 3k and Extended Data Fig. 4d–f). Moreover, it is evident that the outcome can be altered depending on the choice of normalization method (Fig. 3k). These data suggest the need to use more quantitative methods when analysing possible differences in both interregional and intraregional tissue sections, as well as off-tissue validation, if possible.

Next, to investigate the method's potential for absolute quantificative MSI (Q-MSI), we initially determined metabolite concentrations in the unlabelled yeast extract using nuclear magnetic resonance spectroscopy (NMR)[24]. Subsequently, we spotted varying amounts of unlabelled yeast extracts on the slide alongside the tissue before spraying with ^{13}C-labelled yeast extracts (Fig. 4a). The MSI method was optimized to capture all tissue in each spot for MS measurement, enabling calculation of the measured spot volume (Extended Data Fig. 5a). Based on this, a set of calibration lines were constructed for quantification using the obtained response factors (Fig. 4b and Extended Data Fig. 5). Taking brain tissue as an example, the excitatory neurotransmitter aspartate showed a specific quantitative distribution in the cerebellar granular layer of approximately 8 nmol mm^{-3} (Fig. 4c), which is consistent with previous reports claiming that aspartate is a possible neurotransmitter in cerebellar climbing fibres[25]. The average values of eight spatially quantified metabolites showed a strong correlation with the NMR results from bulk tissue samples (Fig. 4d). This absolute quantification enables both interregion comparisons of identical metabolites and intermetabolite comparisons, offering advantages over other normalization methods (Fig. 4d). To compare the absolute quantification values from MSI with NMR results, we

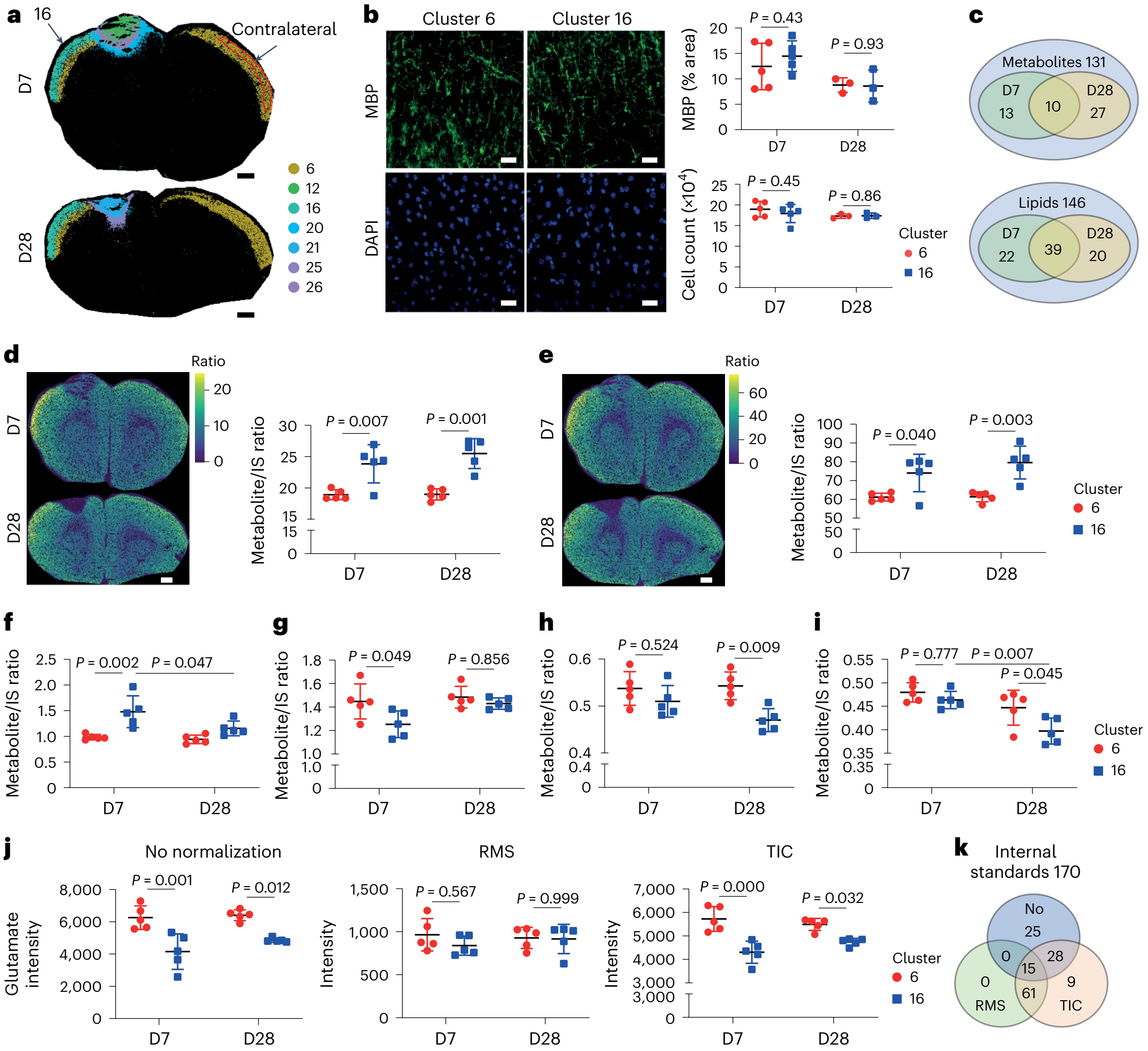

Fig. 3 | Remote metabolic alterations on ipsilateral cortex after ischaemic stroke revealed by quantitative spatial metabolomics. **a**, Spatial segmentation of the infarct and cortex areas. Cluster 16 and its contralateral region in cluster 6 are highlighted. **b**, Left: representative images of myelin (MBP) and DAPI staining on the cortex areas of D7 samples ($n = 5$). Right: comparison of myelin coverage and cell count on different cortex areas of D7 ($n = 5$) and D28 ($n = 3$) samples. Two-tailed Student's *t*-test was performed. **c**, Number of quantified metabolite and lipid features and the significant difference between cluster 16 and its contralateral region in cluster 6. **d**, Left: representative image showing LPE O-16:1 distribution in the post-stroke brains ($n = 5$ per group). Right: relative quantification in clusters 16 and its contralateral region in cluster 6. One-way ANOVA followed by Tukey's HSD test were performed. **e**, Left: representative image showing LPE O-18:1 distribution in the post-stroke brains ($n = 5$ per group). Right: relative quantification in clusters 16 and its contralateral region in cluster 6. One-way ANOVA followed by Tukey's HSD test were performed. Colour bars in (**d**,**e**) indicate ratio of metabolite to internal standard. **f**–**i**, Relative quantification of lysine (**f**), glutamate (**g**), UDP-GlcNAc (**h**) and linoleate (**i**) in cluster 16 and its contralateral region in cluster 6 ($n = 5$ per group). One-way ANOVA followed by Tukey's HSD test were performed. **j**, Relative intensity of glutamate in cluster 16 and its contralateral region in cluster 6 using different normalization methods ($n = 5$ per group). One-way ANOVA followed by Tukey's HSD test were performed. **k**, Number of IS and the significant difference between cluster 16 and its contralateral region in cluster 6 using different normalization methods. All data in plots are presented as mean ± s.d. Scale bars, 20 µm (**a**), 600 µm (**b**,**d**,**e**).

assumed a brain density of 1.03 g cm^{-3}. The MSI quantification values were in a similar range to the NMR results (Fig. 4e). However, MSI values were generally higher, possibly because of differences in the measured areas between MSI and NMR or the presence of isomers or isobars in MSI measurements. In addition, the presence overlapping signals limits the number of metabolites that can be accurately quantified using MSI. One limitation of MALDI-MSI technology is that one cannot separate the isomers or isobars in a omics-scale measurement, which may interfere with the accuracy of quantification or normalization. Moreover, in-source fragmentation remains a major bottleneck of MALDI-MSI analysis. The ^{13}C-labelled yeast extract used here is 99% enriched, which largely prevents the introduction of unlabelled exogenous yeast metabolites; nevertheless, trace unlabelled species may still originate from the IS.

In summary, we introduce an improved quantitative spatial metabolomics approach utilizing ^{13}C-labelled yeast extract as a source of isotopically labelled IS. This method enables both relative quantification with pixelwise IS normalization and absolute spatial quantification. Beyond metabolite IS, the inclusion of IS for lipids significantly enhances the quantification capacity of this method by orders of magnitude[8,26]. Using an experimental stroke model we demonstrate that our advanced quantitative methodology reveals remote regions in the brain that have hitherto evaded histological and molecular imaging with MALDI-MSI techniques. Matrix effects are affected by physico-chemical properties not only in different regions, but also in different (patho-) physiological conditions in similar regions. Thus, the choice of different normalization methods leads to altered outcomes, which is also true for the choice of matrix and MSI technique.

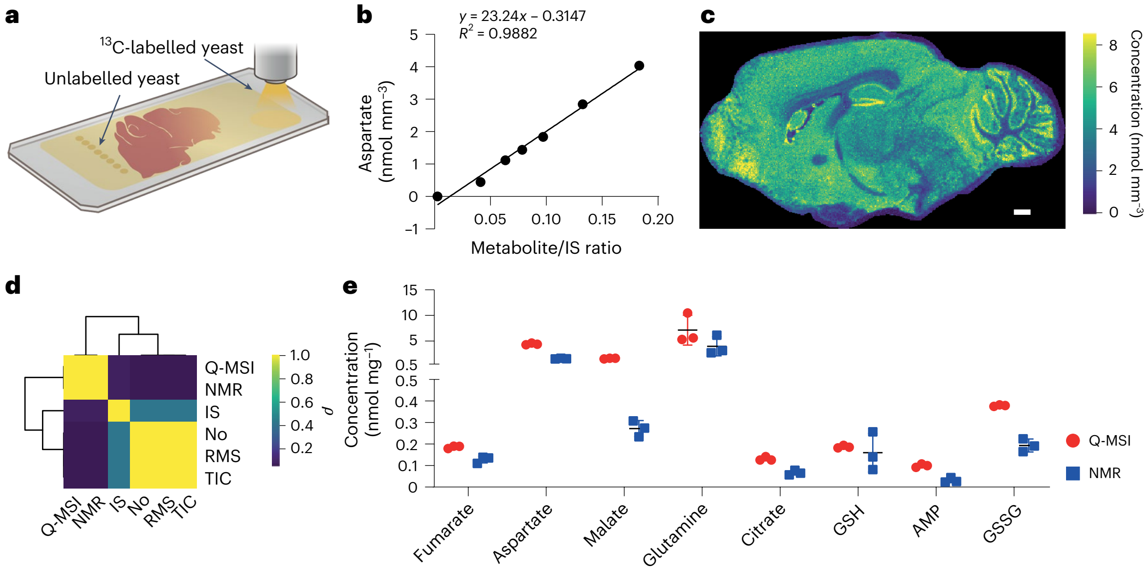

Fig. 4 | ^{13}C yeast-assisted MSI for absolute quantitative spatial metabolomics. **a**, Scheme of absolute quantitative spatial metabolomics. **b**, Calibration line for aspartate quantification. **c**, Absolute spatial quantification of aspartate on mouse brain. **d**, Spearman correlation analysis on the average abundance of eight metabolites detected using different methods. **e**, Comparison of average quantification values between Q-MSI and NMR ($n = 3$) from three different brain samples. Data are presented as mean ± s.d. R^2, coefficient of determination. Scale bar, 600 µm.

For example, MALDI-MSI detection of a homogeneously deposited lipid standard (PE15:0/18:1 (d7)) on brain showed distinct MSI images with unequally distributed peak intensity when comparing norharman or 2,5-dihydroxybenzoic acid as a matrix[8]. Furthermore, MALDI-MSI and DESI-MSI showed opposite pool-size results of long-chain fatty acid palmitate or stearate when comparing tumour relative to healthy tissue regions in a mouse model of glioblastoma[27]. Although we demonstrate our method using NEDC matrix and MALDI-MSI, alternative matrices or other analytical modalities such as DESI-MSI should equally benefit from the presented approach. In essence, this method sets a standard for spatial metabolomics studies, offering improved accuracy and reduced batch effects.

Methods

Mouse studies

Mouse kidneys were obtained from normal 12-week-old male DBA/2J mice ($n = 3$). Animal experiments were approved by the Ethical Committee on Animal Care and Experimentation at Leiden University Medical Center (Permit No. AVD1160020172926). Control mouse brains were obtained from normal 12-week-old male C57BL/6J mice ($n = 3$). Animal experiments were approved by the Ethical Committee on Animal Care and Experimentation at Leiden University Medical Center (Permit No. AVD11600202316801). Mice were perfused with cold phosphate-buffered saline (PBS)–heparin (5 IU ml^{-1}) via the left ventricle at a controlled pressure of 150 mmHg for 6 min to exsanguinate the kidneys or brains before removal. All tissues were quenched with liquid nitrogen and stored at −80 °C. All work with animals was performed in compliance with Dutch government guidelines. Mice were housed at 20–22 °C in individually ventilated cages, humidity controlled (55%) with free access to food and water and a light–dark cycle of daytime (6.30 a.m. to 6.00 p.m.) and night-time (6.00 p.m. to 6.30 a.m.).

For brain stroke experiments, all animal procedures were performed in accordance with guidelines for the use of experimental animals and were approved by the respective governmental committees (Regierungspraessidium Oberbayern, the Rhineland Palatinate Landesuntersuchungsamt Koblenz). Wild-type C57BL6/J mice were purchased from Charles River. Wild-type male mice (aged 12–13 weeks) were used for the experiments. All mice had free access to food and water with a 12 h dark–light cycle and were housed under a controlled temperature (22 ± 2 °C). All animal experiments were performed and reported in accordance with the Animal Research: Reporting In Vivo Experiments (ARRIVE) guidelines.

Photothrombosis experimental stroke surgery

For photothrombosis induction, ten mice were randomly divided into two groups ($n = 5$ per group). Mice were anaesthetised with isoflurane, delivered in a mixture of 30% O_2 and 70% N_2O, and then placed in a stereotactic frame. Body temperature was maintained at 37 °C with a warming pad. Dexpanthenol eye ointment was applied to both eyes. Animals received 10 µl per g of body weight of 1% Rose Bengal (Sigma-Aldrich, catalogue no. 198250-5g) in saline by intraperitoneal injection 5 min before induction of anaesthesia (5% isoflurane). A skin incision was made to expose the skull. Bregma was located and the laser collimator was set at 1 mm diameter and placed over the lesion location (1.5 mm lateral and 1.0 mm rostral to bregma). Ten minutes after Rose Bengal injection the laser (25 mV output) was applied to the lesion area for 17 min (Cobolt Jive 50, 561 nm power; Fiber Collimation Package: 543 nm).

Mice were killed by anaesthetizing with ketamine (120 mg kg^{-1}) and xylazine (16 mg kg^{-1}). Mice were then transcardially perfused with 0.9% NaCl and the brain was carefully excised and immediately frozen on dry ice. Brain cryostat sections were cut at 10 µm for MSI and 20 µm for immunohistochemistry, and were mounted directly on glass slides and stored at −80 °C.

Immunohistochemistry

For immunohistochemical analysis of MBP and 4′,6-diamidino-2-phenylindole (DAPI), tissue was fixed on slides with 4% paraformaldehyde for 20 min at room temperature, followed by three washes of 1× PBS. Tissue was permeabilized and blocked for 1 h at room temperature in 1× PBS containing 2% goat serum (Thermo Fisher Scientific, catalogue no. 16210-064), 2% bovine serum albumin (Sigma-Aldrich, A3912) and 0.2% Triton X-100 (Sigma-Aldrich, X100). Sections were then immunolabeled with MBP (1:200; Bio-Rad, MAB386) for 24 h at 4 °C. After primary antibody labelling, sections were washed three times in

1× PBS for 10 min at room temperature and incubated with fluorescent secondary antibody (Alexa Fluor 488 goat anti-rat; Invitrogen, A11006) for 2 h at room temperature. Sections were washed three times in 1× PBS for 10 min at room temperature and incubated with DAPI (Invitrogen, D1306) for 5 min at room temperature, then washed three more times in 1× PBS for 10 min at room temperature and sealed with coverslips using Fluoromount medium (Sigma-Aldrich, catalogue no. F4680).

Confocal microscopy acquisition and image analysis

All images were taken on a Zeiss LSM 880 confocal imaging system with a ×40 water immersion objective. Z-stacks were taken at 1-µm intervals at three regions along layers II–III of the cortex per hemisphere. Coverage analysis was performed using the 'Particle Analysis' function in Image J. The percentage area of three images per hemisphere was then averaged.

To quantify cell count, DAPI was used to manually count the nuclei in Image J using the 'Multi-point' function. The cell counts for the three regions imaged per hemisphere were then averaged.

Internal standard and matrix application

Tissues were embedded in 10% gelatine and cryosectioned into 10-µm-thick sections using a Cryostar NX70 cryostat (Thermo Fisher Scientific) at −20 °C. The sections were thaw-mounted onto glass slides coated with indium tin oxide (VisionTek Systems). Mounted sections were placed in a vacuum freeze-dryer for 15 min before matrix application. After drying, the tissue slices on indium tin oxide slides were heated to approximately 80 °C for 15 s on a hot plate to denature metabolic enzymes.

Unlabelled metabolite yeast extracts (ISO1-UNL, Cambridge Isotope Laboratories) and U-^{13}C-labelled metabolite yeast extracts (99%; ISO1, Cambridge Isotope Laboratories) were reconstituted in 2 ml of 50% methanol–deionized water. The mixtures were shaken by hand with intermittent high-speed vortexing for a minimum of 2 min, followed by centrifugation at 20 °C and 4,000*g* for 5 min. The clear standard solutions were collected and stored at −80 °C.

For IS applications, the ^{13}C-labelled yeast extract solution was diluted in methanol (1:10 v/v). IS were then sprayed onto the tissue surface using a HTX M3+ Sprayer (HTX Technologies). The setting for IS application was: temperature, 60 °C; flow rate, 80 µl min^{-1}; velocity, 1,200 mm min^{-1}; track spacing, 2 mm; gas flow rate 10 pounds per square inch; drying time between passes, 10 s. Kidney and stroke brain tissues underwent 70 layers of passes. For absolute quantitative analysis on normal mouse brain tissues, eight varying amounts of unlabelled yeast extracts were spotted alongside the brain tissue slices before the spray of ^{13}C-labelled yeast extracts. Two replicates were spotted for each concentration. Then 70 layers of IS were sprayed on both brain tissues ($n = 3$) and spots of unlabelled yeast extracts.

Following application of IS, an NEDC (Sigma-Aldrich) MALDI-matrix solution of 7 mg ml^{-1} in methanol–acetonitrile–deionized water (70:25:5 v/v/v) was applied using a HTX M3+ Sprayer (HTX Technologies). The setting was: temperature, 60 °C; number of passes, 20 layers; flow rate, 80 µl min^{-1}; velocity, 2,000 mm min^{-1}; track spacing, 3 mm; gas flow rate 10 p.s.i.; drying time between passes, 30 s.

MALDI-MSI measurement

MALDI-MSI was performed using a TimsTOF MALDI2 system (Bruker Daltonics). The instrument was calibrated using red phosphorus before each measurement. All the data were acquired in negative mode with MALDI2 at a mass range of m/z 50–1,000. The MALDI2 laser had a pulse delay time of 10 µs. For kidney and brain stroke tissues, data were acquired at a pixel size of 20 µm (x, y) using a beam scan area of 16 × 16 µm and laser was operated at 1 kHz with 200 laser shots accumulated per pixel. For absolute quantitative analysis on brain tissues, data were acquired at a pixel size of 30 µm (x, y) using a beam scan area of 26 × 26 µm and laser was operated at 1 kHz with 100 laser shots accumulated per pixel. Data acquisition was performed using flexControl (v.4.0, Bruker Daltonics). All the samples from same slides were measured randomly.

Quantification of metabolites from unlabelled yeast extract by NMR

An aliquot of unlabelled yeast extract was prepared in 0.05 M phosphate buffer in 99.8% deuterated water including 0.05 mM of trimethylsilyl propionic-d4-sodium salt as a reference and quantification standard[24]. A 185 µl aliquot was transferred to a 3-mm NMR tube and one NMR experiment (pulse sequence: noesygppr1d; Bruker Biospin) was collected in a 14.1 T (600 MHz for 1H) Bruker Avance Neo NMR. Yeast metabolites were then quantified using the Chenomx NMR suite 10.0 software (Chenomx NMR suite, v.10.0). The identities of the metabolites were confirmed by two-dimensional NMR (^{1}H–^{1}H total correlation spectroscopy and ^{1}H–^{13}C heteronuclear single quantum coherence) experiments.

Untargeted LC–MS–MS metabolomics

Normal kidney and brain samples stored at −80 °C were thawed on ice. The thawed sample was homogenized in a grinder (30 Hz) for 20 s. A 400 µl extraction solution (methanol–water, 7:3 v/v) containing IS was added to 20 mg of homogenized tissue, shaken and centrifuged at 1,500*g* for 5 min. After placing on ice for 15 min, the sample was centrifuged at 12,000*g* for 10 min (4 °C). Then 300 µl of supernatant was collected and placed at −20 °C for 30 min. The sample was centrifuged again at 12,000*g* for 3 min (4 °C). Finally, a 200 µl aliquot of supernatant was transferred for LC–MS analysis.

Unlabelled yeast extract stored at −80 °C was thawed on ice and vortexed for 10 s. Then 150 µl of extraction solution (acetonitrile–methanol, 1:4 v/v) containing IS was added to 50 µl of the sample. The mixture was vortexed for 3 min and centrifuged at 12,000*g* for 10 min (4 °C). A 150 µl aliquot of the supernatant was collected, kept at −20 °C for 30 min, and centrifuged at 12,000*g* for 3 min (4 °C). An 120-µl aliquot of the supernatant was transferred for LC–MS analysis.

Samples were analysed using two LC–MS methods. One aliquot was analysed by positive mode electrospray ionization using a T3 column (Waters ACQUITY Premier HSS T3 Column 1.8 µm, 2.1 × 100 mm) with 0.1% formic acid in water as solvent A and 0.1% formic acid in acetonitrile as solvent B. The following gradient was used: 5% to 20% in 2 min, increased to 60% in the following 3 min, increased to 99% in 1 min and held for 1.5 min; returned to 5% mobile phase B within 0.1 min and held for 2.4 min. The column oven was kept at 40 °C, the flow rate was 0.4 ml min^{-1} and the injection volume was 4 µl. The second aliquot was analysed in negative mode electrospray ionization mode under identical conditions.

The mass spectrometer was operated with data acquisition performed in information-dependent acquisition mode using Analyst TF v.1.7.1 software (Sciex). The source parameters were set as follows: ion source gas 1, 50 p.s.i.; ion source gas 2, 50 p.s.i.; curtain gas, 25 p.s.i.; temperature, 550 °C; declustering potential, 60 V or −60 V in positive or negative mode, respectively; and ion spray voltage floating, 5,000 V or −4,000 V in positive or negative modes, respectively. The time of flight MS scan parameters were: mass range, 50–1,000 Da; accumulation time, 200 ms; dynamic background subtract, on. The product ion scan parameters were set as: mass range, 25–1,000 Da; accumulation time, 40 ms; collision energy, 30 V or −30 V in positive or negative modes, respectively; collision energy spread, 15; resolution, UNIT; charge state, 1 to 1; intensity, 100 counts per second; exclude isotopes within 4 Da; mass tolerance, 50 ppm; maximum number of candidate ions to monitor per cycle, 18.

Untargeted LC–MS–MS lipidomics

Kidney and brain samples stored at −80 °C were thawed on ice. Then 20 mg of thawed sample was homogenized in a grinder (30 Hz) for 20 s and centrifuged (3,000*g*, 4 °C) for 30 s. Unlabelled yeast extract stored at −80 °C was thawed on ice and vortexed for 10 s. The tissue extract or 200 µl of the yeast extract were mixed with 1 ml of extraction solvent (*tert*-butyl methyl ether–methanol, 3:1 v/v) containing the IS mixture. After the mixture had been vortexed for 15 min, 200 µl of ultrapure water was added, followed by vortexing for 1 min and centrifugation at 12,000*g* for 10 min. Then 200 µl of the upper organic layer was collected and evaporated using a vacuum concentrator. The dry extract was dissolved in 200 µl of reconstituted solution (acetonitrile–isopropanol, 1:1 v/v).

The sample extracts were analysed using an liquid chromatography–electrospray ionization–tandem mass spectrometry system (UPLC, ExionLC AD; MS, QTRAP 6500+ system). A Thermo Accucore C30 (2.6 µm, 2.1 mm × 100 mm internal diameter) was used with the following analytical conditions: solvent A, acetonitrile–water (60:40 v/v, 0.1% formic acid, 10 mmol l^{-1} ammonium formate); solvent B, acetonitrile–isopropanol (10:90 v/v, 0.1% formic acid, 10 mmol l^{-1} ammonium formate); gradient programme, A–B (80:20, v/v) at 0 min, 70:30 v/v at 2.0 min, 40:60 v/v at 4 min, 15:85 v/v at 9 min, 10:90 v/v at 14 min, 5:95 v/v at 15.5 min, 5:95 v/v at 17.3 min, 80: 20 v/v at 17.3 min and 80:20 v/v at 20 min; flow rate, 0.35 ml min^{-1}; temperature, 45 °C; injection volume, 2 µl.

A QTRAP 6500+ system was used for mass spectrometric read out. The LC–MS–MS system was equipped with an electrospray ionization turbo ion spray interface, operating in positive and negative ion mode, controlled by Analyst v.1.6.3 software (Sciex). The electrospray ionization source operation parameters were as follows: ion source, turbo spray; source temperature, 500 °C; ion spray voltage, 5,500 V (positive) and −4,500 V (negative); ion source gas 1, gas 2 and curtain gas were set at 45 p.s.i., 55 p.s.i. and 35 p.s.i., respectively. Instrument tuning and mass calibration were performed with 10 and 100 µmol l^{-1} polypropylene glycol solutions in triple quadrupole and linear ion trap modes, respectively. Triple quadrupole scans were acquired as multiple reaction monitoring (MRM) experiments with collision gas (nitrogen) set to 5 p.s.i. Declustering potential and collision energy for individual MRM transitions was done with further declustering potential and collision energy optimization. A specific set of MRM transitions were monitored for each period according to the metabolites eluted within this period.

MSI data processing and analysis

MSI data were imported and processed in SCiLS Lab 2023c Pro (SCiLS, Bruker Daltonics). Peak picking was performed on the average spectrum with a threshold signal-to-noise ratio >3 and relative intensity >0.01% in mMass[28]. In addition, peaks that appeared only in the matrix sample were excluded from the *m*/*z* feature list and further analysis. The resulting *m*/*z* features from the unlabelled yeast extract were then compared with an annotated LC–MS–MS dataset from an aliquot of the same yeast extract and pre-annotated with an error of less than ±10 ppm. The *m*/*z* features that were not found in the LC–MS–MS dataset were further imported into the Yeast Metabolome Database[29] and Human Metabolome Database[30] for potential pre-annotation with an error of less than ±10 ppm. Lipid *m*/*z* values from unlabelled yeast extract were imported into the LIPID MAPS database[31] and pre-annotated with an error of less than ±10 ppm. Odd-chain lipids were removed because they usually are minor components in mammals. Most of the pre-annotated metabolites and lipids were further confirmed using the product certificate from the supplier. For kidneys and brain tissues, peaks overlapping with ^{13}C-labelled yeast extract, but not with the control tissue, were removed. In summary, selected *m*/*z* values were pre-annotated using the following strategy: (1) database search using high-resolution masses against the Human Metabolome Database, and LIPID MAPS database with an error of less than ±10 ppm; (2) validation of the so generated hits by off-tissue LC–MS–MS analysis; and (3) comparison with a previously published dataset[32] to further verify the pre-annotations.

Following annotation of the *m*/*z* features of the unlabelled yeast extract, the corresponding theoretical *m*/*z* values of the U-^{13}C-labelled metabolites and lipids were calculated to facilitate search of the experimental *m*/*z* features from ^{13}C-enriched metabolites. Any peak from U-^{13}C-labelled yeast extract overlapping with peaks of unlabelled yeast extracts was removed from further analysis. The *m*/*z* values of U-^{13}C-labelled yeast extract after peak picking were further compared with the calculated theoretical *m*/*z* value of the uniformly ^{13}C-labelled metabolites and lipids. The U-^{13}C-labelled metabolites and lipids found in ^{13}C-labelled yeast extract were pre-annotated with an error of less than ±10 ppm. IS pairs were established containing unlabelled metabolic features and their U-^{13}C-labelled counter parts, which were used for the subsequent analysis of brain and kidney tissues. (Supplementary Table 1).

Peaks from kidney or brain tissues matching the IS were selected for further analysis (Supplementary Table 2). An additional layer of control included removal of overlapping ^{13}C-labelled signals with endogenous tissue signals. The final set of IS pairs was used for pixelwise normalization on both kidney and brain tissues. IS pairs were used for relative quantification of their paired unlabelled metabolic features on tissues by calculating the ratio of unlabelled metabolic features to IS. The selected lipid IS with highest peak intensity were used for relative quantification of eight different lipid classes (Supplementary Table 3). The pixelwise normalization to IS was performed by calculating unlabelled metabolic feature to IS ratio. Pixels that contain a missing value '0' on each IS were removed for further analysis.

For absolute quantitative spatial metabolomics analysis, seven different amounts of unlabelled yeast extracts (0, 1, 2, 3, 4, 6 and 8 µl) were diluted to 10 µl, and 1 µl of each dilution was spotted next to the tissue sections with two replicates for each concentration. ^{13}C-labelled yeast extract was sprayed over both the yeast spots and the tissue section, and the unlabelled yeast spots and tissue sections were then measured by MSI in the same run as described above. The absolute amount of the metabolites on each spot was calculated based on NMR measurement (Supplementary Table 5) and the obtained concentration was divided by the number of pixels in the spot to determine the amount per pixel. The ratio of the signal from the unlabelled metabolite to that of the ^{13}C-labelled metabolite from the spotted yeast extracts was then used to generate calibration lines with individual equations for each metabolite using GraphPad Prism 9. The equations were further used for absolute quantification in each pixel from the tissues. For tissue, the volume of each pixel was defined as 30 × 30 × 10 μm^3, which was used to convert the per-pixel amount to a concentration expressed in nanomoles per cubic millimetre.

The *m*/*z* features of endogenous lipid features or *m*/*z* features of exogenous metabolites and lipids were selected manually in SCiLS Lab 2016b for UMAP analysis. Their intensities were exported for all the measured pixels with RMS normalization from SCiLS Lab 2016b. The datasets were transformed into a count matrix by taking the integer part. This count data matrix was normalized and scaled using SCTransform to generate a two-dimensional UMAP map using Seurat[33] in R. The distributions of the pixels from different clusters on tissues were co-registered to the post-MSI staining, and regions were identified based on both staining and their morphology. For the stroke study, the region information of each pixel was used to calculate the average abundance of both the endogenous metabolic feature and IS for regional comparison. For cluster 16, its contralateral regions in cluster 6 were selected manually in SCiLS Lab 2023c Pro after co-registering with the cluster distribution (Fig. 2g). The average abundance of both metabolic features and IS from cluster 16 and its contralateral region were exported from SCiLS Lab 2023c Pro for further comparison. The code used in this part is similar to that in GitHub (https://github.com/Gangqiwang/scDYMO).

For molecular histology, the datasets were used to generate a three-dimensional UMAP map using packages Seurat 4.3 and plotly. The embedding information of the three-dimensional UMAP was translated to RGB colour coding by varying red, green and blue intensities on the three independent axes. Together with pixel coordinate information exported from SCiLS Lab 2023c Pro, a MxNx3 data matrix was generated and used to generate UMAP images in MATLAB R2019a. The code used in this part is similar to that in GitHub (https://github.com/Gangqiwang/scDYMO).

Data collection and analysis were not performed blind to the conditions of the experiments.

Statistics and reproducibility

No statistical methods were used to predetermine sample sizes, which were similar to those reported in previous publications[13]. All experiments and data analysis were performed on three or five animals per group. No animals or data points were excluded from the analysis. All data are presented as mean ± s.d., unless indicated otherwise. Data normality and equal variances were tested using the Shapiro–Wilk test. Differences between more than three groups were assessed by one-way analysis of variance (ANOVA) test following by Tukey's honest significance test (HSD) test. Differences between two groups were assessed by two-tailed Student's t-test, or by two-tailed F-test when the distribution of measurements was not normal. A P value <0.05 was considered statistically significant.

Reporting summary

Further information on research design is available in the Nature Portfolio Reporting Summary linked to this article.

Data availability

Because of the large size of all raw data, the exported and processed MSI data are available at Figshare (https://doi.org/10.6084/m9.figshare.28665017.v1)[34], to provide the necessary information spectrum quality. For full availability of raw MALDI-MSI data related to this study, please contact G.W. (g.wang@lumc.nl) or M.G. (m.a.giera@lumc.nl) and data will be made available upon reasonable request. Source data are provided with this paper.

References

1. Vandereyken, K., Sifrim, A., Thienpont, B. & Voet, T. Methods and applications for single-cell and spatial multi-omics. *Nat. Rev. Genet.* **24**, 494–515 (2023).
2. Ma, S. Y. et al. High spatial resolution mass spectrometry imaging for spatial metabolomics: advances, challenges, and future perspectives. *Trends. Analyt. Chem.* **159**, 116902 (2023).
3. Tobias, F. & Hummon, A. B. Considerations for MALDI-based quantitative mass spectrometry imaging studies. *J. Proteome Res.* **19**, 3620–3630 (2020).
4. Lanekoff, I., Stevens, S. L., Stenzel-Poore, M. P. & Laskin, J. Matrix effects in biological mass spectrometry imaging: identification and compensation. *Analyst* **139**, 3528–3532 (2014).
5. Taylor, A. J., Dexter, A. & Bunch, J. Exploring ion suppression in mass spectrometry imaging of a heterogeneous tissue. *Anal. Chem.* **90**, 5637–5645 (2018).
6. Matuszewski, B. K., Constanzer, M. L. & Chavez-Eng, C. M. Strategies for the assessment of matrix effect in quantitative bioanalytical methods based on HPLC-MS/MS. *Anal. Chem.* **75**, 3019–3030 (2003).
7. Balluff, B., Hopf, C., Porta Siegel, T., Grabsch, H. I. & Heeren, R. M. A. Batch effects in MALDI mass spectrometry imaging. *J. Am. Soc. Mass. Spectrom.* **32**, 628–635 (2021).
8. Vandenbosch, M. et al. Toward omics-scale quantitative mass spectrometry imaging of lipids in brain tissue using a multiclass internal standard mixture. *Anal. Chem.* **95**, 18719–18730 (2023).
9. Cífková, E. et al. Nontargeted quantitation of lipid classes using hydrophilic interaction liquid chromatography–electrospray ionization mass spectrometry with single internal standard and response factor approach. *Anal. Chem.* **84**, 10064–10070 (2012).
10. Wasito, H. et al. Yeast-based reference materials for quantitative metabolomics. *Anal. Bioanal. Chem.* **414**, 4359–4368 (2022).
11. Mashego, M. R. et al. MIRACLE: mass isotopomer ratio analysis of U-^{13}C-labeled extracts. A new method for accurate quantification of changes in concentrations of intracellular metabolites. *Biotechnol. Bioeng.* **85**, 620–628 (2004).
12. Chumbley, C. W. et al. Absolute quantitative MALDI imaging mass spectrometry: a case of rifampicin in liver tissues. *Anal. Chem.* **88**, 2392–2398 (2016).
13. Wang, G. et al. Analyzing cell-type-specific dynamics of metabolism in kidney repair. *Nat. Metab.* **4**, 1109–1118 (2022).
14. Llovera, G., Pinkham, K. & Liesz, A. Modeling stroke in mice: focal cortical lesions by photothrombosis. *J. Vis. Exp.* **171**, e62536 (2021).
15. Medoh, U. N. et al. The Batten disease gene product CLN5 is the lysosomal *bis*(monoacylglycero)phosphate synthase. *Science* **381**, 1182–1188 (2023).
16. Bulfon, D. et al. Functionally overlapping intra- and extralysosomal pathways promote *bis*(monoacylglycero) phosphate synthesis in mammalian cells. *Nat. Commun.* **15**, 9937 (2024).
17. Xu, Z. Q. et al. Alterations in metabolome and lipidome in patients with in-stent restenosis. *CNS Neurosci. Ther.* **30**, e14832 (2024).
18. Hennebelle, M. et al. Linoleic acid participates in the response to ischemic brain injury through oxidized metabolites that regulate neurotransmission. *Sci. Rep.* **7**, 4342 (2017).
19. Hisano, K. et al. Structurally different lysophosphatidylethanolamine species stimulate neurite outgrowth in cultured cortical neurons via distinct G-protein-coupled receptors and signaling cascades. *Biochem. Biophys. Res. Commun.* **534**, 179–185 (2021).
20. Lai, K. et al. Glutamate acts on acid-sensing ion channels to worsen ischaemic brain injury. *Nature* **631**, 826–834 (2024).
21. Kondoh, T., Kameishi, M., Mallick, H. N., Ono, T. & Torii, K. Lysine and arginine reduce the effects of cerebral ischemic insults and inhibit glutamate-induced neuronal activity in rats. *Front. Integr. Neurosci.* **4**, 18 (2010).
22. Li, X. & Yang, W. Targeting O-GlcNAcylation in ischemic stroke. *Neural Regen. Res.* **17**, 2427–2428 (2022).
23. Iso, H. et al. Linoleic acid, other fatty acids, and the risk of stroke. *Stroke* **33**, 2086–2093 (2002).
24. Kostidis, S., Addie, R. D., Morreau, H., Mayboroda, O. A. & Giera, M. Quantitative NMR analysis of intra-and extracellular metabolism of mammalian cells: a tutorial. *Anal. Chim. Acta* **980**, 1–24 (2017).
25. Wiklund, L., Toggenburger, G. & Cuenod, M. Aspartate: possible neurotransmitter in cerebellar climbing fibers. *Science* **216**, 78–80 (1982).
26. Ejsing, C. S. et al. Global analysis of the yeast lipidome by quantitative shotgun mass spectrometry. *Proc. Natl Acad. Sci. USA* **106**, 2136–2141 (2009).
27. Schwaiger-Haber, M. et al. Using mass spectrometry imaging to map fluxes quantitatively in the tumor ecosystem. *Nat. Commun.* **14**, 2876 (2023).
28. Strohalm, M., Kavan, D., Novak, P., Volny, M. & Havlicek, V. mMass 3: a cross-platform software environment for precise analysis of mass spectrometric data. *Anal. Chem.* **82**, 4648–4651 (2010).
29. Ramirez-Gaona, M. et al. YMDB 2.0: a significantly expanded version of the yeast metabolome database. *Nucleic Acids Res.* **45**, D440–D445 (2017).
30. Wishart, D. S. et al. HMDB 5.0: the human metabolome database for 2022. *Nucleic Acids Res.* **50**, D622–D631 (2022).
31. Sud, M. et al. LMSD: LIPID MAPS structure database. *Nucleic Acids Res.* **35**, D527–D532 (2007).

32. Lu, W. Y. et al. Acidic methanol treatment facilitates matrix-assisted laser desorption ionization-mass spectrometry imaging of energy metabolism. *Anal. Chem.* **95**, 14879–14888 (2023).
33. Hao, Y. H. et al. Dictionary learning for integrative, multimodal and scalable single-cell analysis. *Nat. Biotechnol.* **42**, 293–304 (2024).
34. Wang, G. Spatial lipidomics datasets on brain stroke samples measured by MALDI-MSI. *figshare* https://doi.org/10.6084/m9.figshare.28665017.v1 (2025).

Acknowledgements

T.J.R. is supported by the Novo Nordisk Foundation Center for Stem Cell Medicine (reNEW, supported by Novo Nordisk Foundation grant no. NNF21CC0073729) and is funded by ERC grant no. SPARK 101140863.

Author contributions

G.W. designed the research study, conducted experiments, processed data and wrote the paper. B.M.v.d.B. performed the animal experiments and gave comments. S.K. performed the NMR experiments, processed data and gave comments. K.P. and A.L. provided the mouse stroke samples, performed the IF staining and gave comments. M.E.J. performed the post-MSI staining and gave comments. M.G. designed the research study and wrote the paper. T.J.R. organized funding, designed the research study and wrote the paper.

Competing interests

The authors declare no competing interests.

Additional information

Extended data is available for this paper at https://doi.org/10.1038/s42255-025-01340-8.

Supplementary information The online version contains supplementary material available at https://doi.org/10.1038/s42255-025-01340-8.

Correspondence and requests for materials should be addressed to Gangqi Wang, Martin Giera or Ton J. Rabelink.

Peer review information *Nature Metabolism* thanks Maryam Faiz, Ramon Sun and the other, anonymous, reviewer(s) for their contribution to the peer review of this work. Primary Handling Editor: Alfredo Giménez-Cassina, in collaboration with the *Nature Metabolism* team.

Reprints and permissions information is available at www.nature.com/reprints.

---

[1]Children's Hospital of Fudan University and the Shanghai Key Laboratory of Medical Epigenetics, Institutes of Biomedical Sciences, Fudan University, Shanghai, China. [2]Department of Internal Medicine (Nephrology) & Einthoven Laboratory of Vascular and Regenerative Medicine, Leiden University Medical Center, Leiden, The Netherlands. [3]The Novo Nordisk Foundation Center for Stem Cell Medicine (reNEW), Leiden University Medical Center, Leiden, The Netherlands. [4]Center of Proteomics and Metabolomics, Leiden University Medical Center, Leiden, The Netherlands. [5]Institute for Stroke and Dementia Research (ISD), University Hospital, LMU Munich, Munich, Germany. [6]Munich Cluster for Systems Neurology (SyNergy), Munich, Germany. ✉e-mail: g.wang@lumc.nl; m.a.giera@lumc.nl; a.j.rabelink@lumc.nl

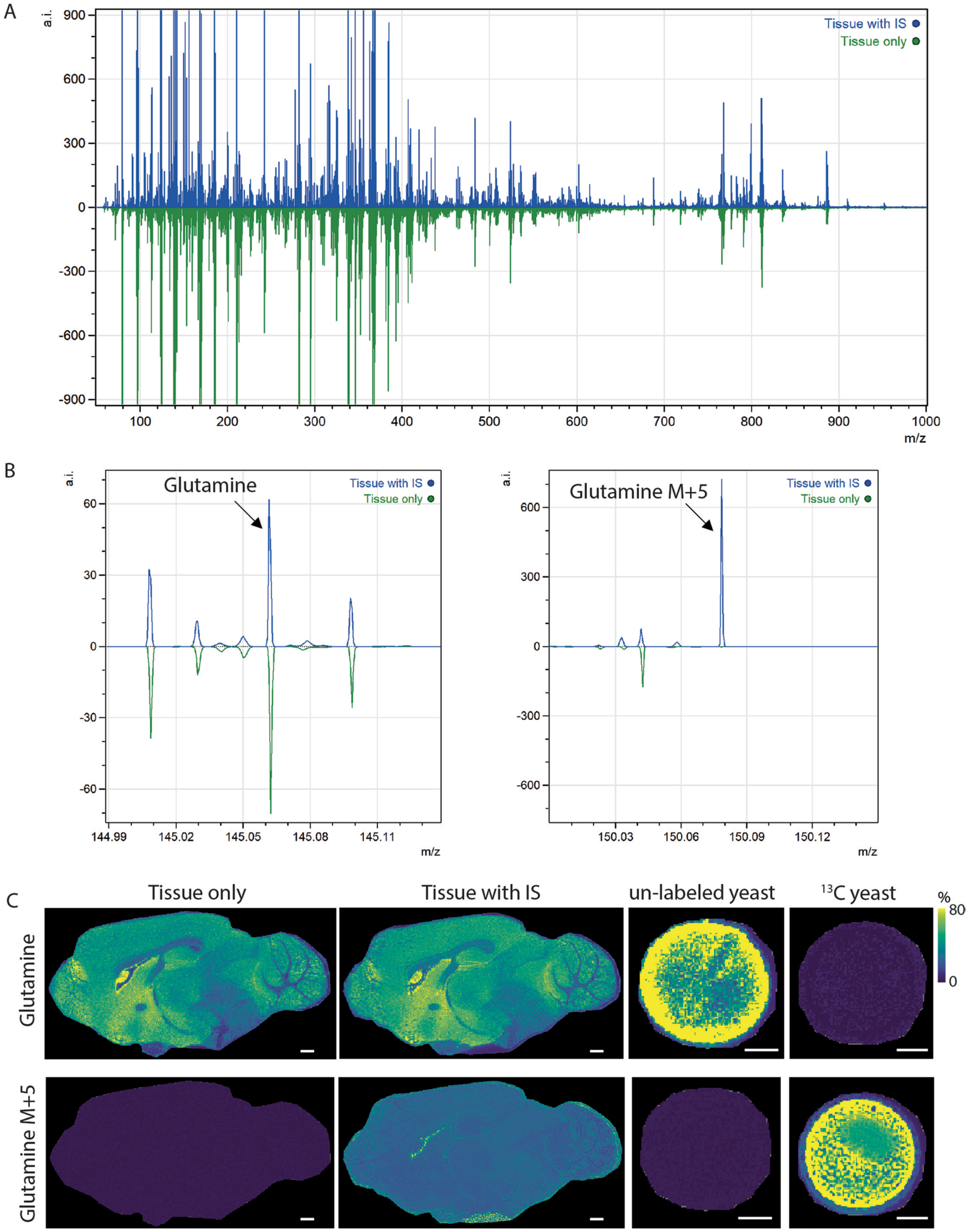

Extended Data Fig. 1 | Spectrum for 13 C yeast-assisted mass spectrometry. **a**, Comparison of spectra from kidney tissues sprayed with and without 13C-labelled yeast extract. **b**, Glutamine peaks from spectra of kidney tissue sprayed with and without 13C-labelled yeast extract. **c**, Comparison of glutamine distribution from brain tissues sprayed with and without 13C-labelled yeast extract and spotted different yeast extracts. All scale bars, 600 µm.

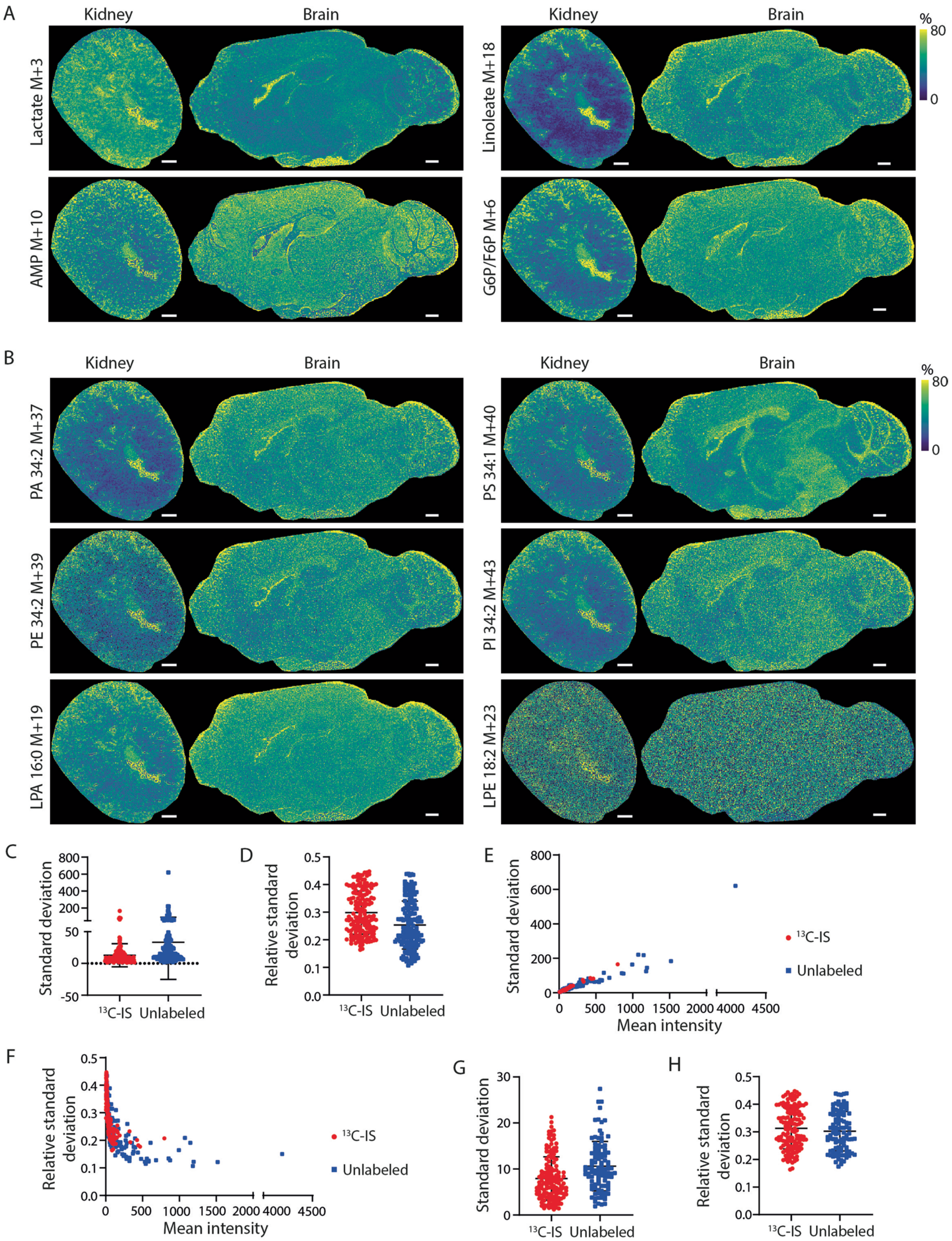

Extended Data Fig. 2 | Ion suppression of different metabolites on both kidney and brain. a, Distribution of different metabolite IS from 13C-labelled yeast extract sprayed on both kidney and brain tissues. **b**, Distribution of IS representing 6 lipids classes from 13C-labelled yeast extracts sprayed on both kidney and brain tissues. **c**-**d**, Comparison of standard deviation C and relative standard deviation D of exogenous 13C-labelled yeast extracts (13C-IS, n = 170) with endogenous metabolic features (n = 170) on selected homogenous area on brain. Each dot represents the average value of one metabolic feature from three samples. Data are presented as mean values +/- SD. (**e**-**f**), Correlation of standard deviation E and relative standard deviation F with mean intensity. **g**-**h**, Comparison of standard deviation **g** and relative standard deviation **h** of exogenous 13C-IS (n = 145) with endogenous metabolic features (n = 102) on selected homogenous area on brain with mean intensity lower than 100. Each dot represents the average value of one metabolic feature from three samples. Data are presented as mean values +/- SD. All scale bars, 600 µm.

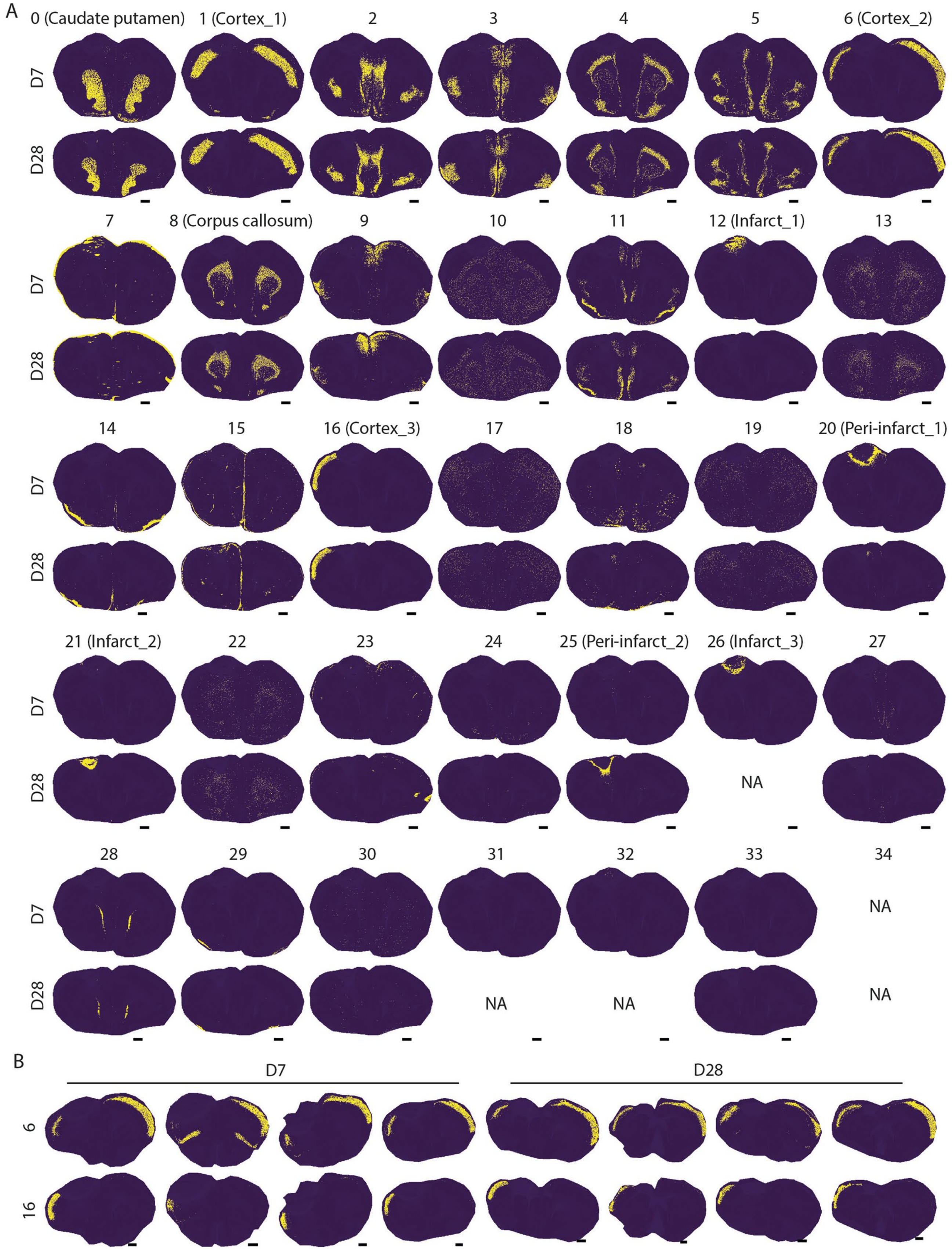

Extended Data Fig. 3 | Spatial distribution of different clusters. a, Representative images of spatial distribution of different UMAP clusters from ischaemic stroke brain based on lipid profile analysis. **b**, Images showing distribution of cluster 6 and 16 in different samples. All scale bars, 600 µm.

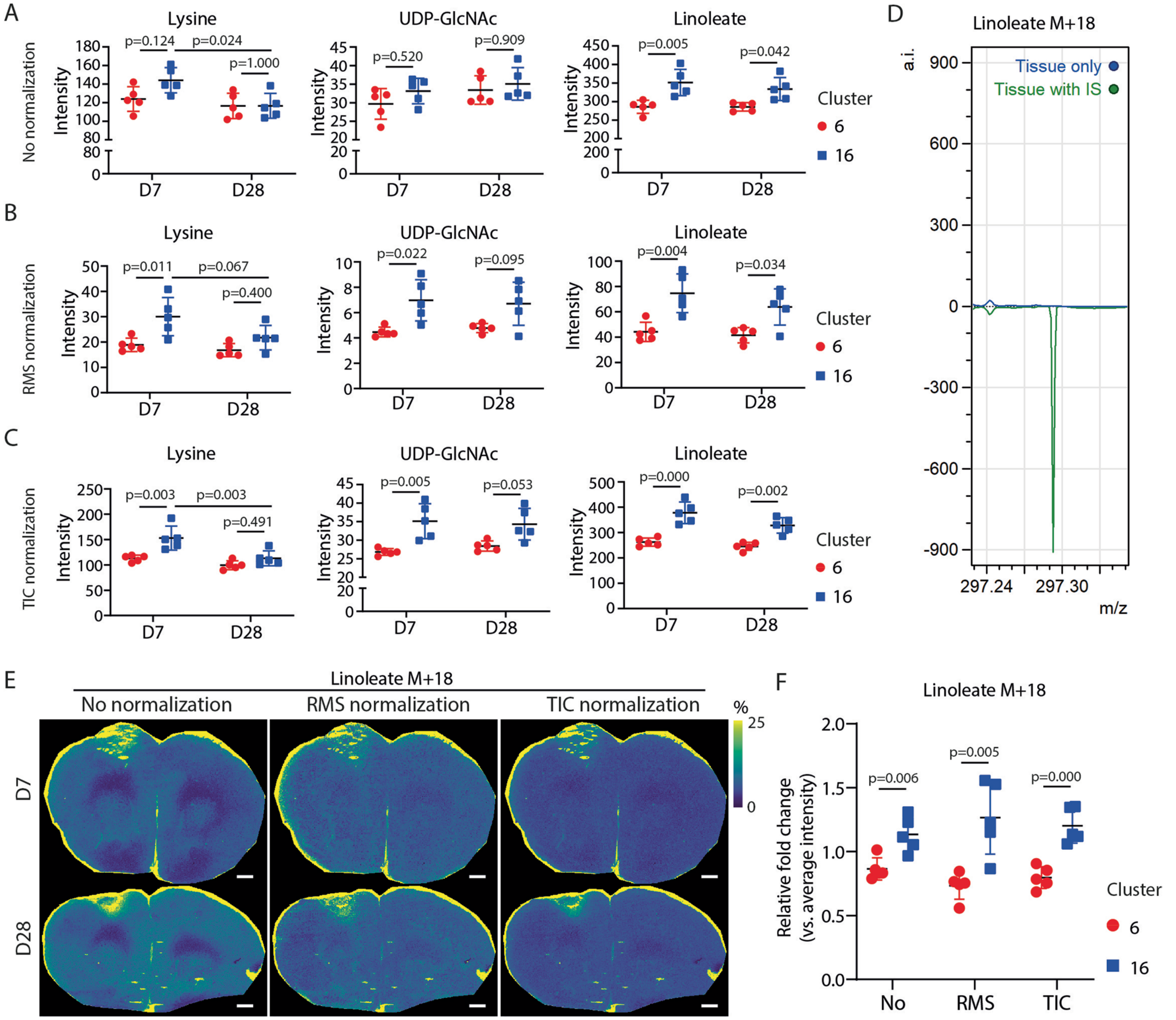

Extended Data Fig. 4 | Comparison of three traditional normalization methods. a, Relative peak intensity of different metabolites in clusters 16 and its contralateral region within cluster 6 without normalization (n = 5 per group). One-way ANOVA test followed by TukeyHSD test were performed. **b**, Relative peak intensity of different metabolites in clusters 16 and its contralateral region within cluster 6 using RMS normalization (n = 5 per group). One-way ANOVA test followed by TukeyHSD test were performed. **c**, Relative peak intensity of different metabolites in clusters 16 and its contralateral region within cluster 6 using TIC normalization (n = 5 per group). One-way ANOVA test followed by TukeyHSD test were performed. **d**, Comparison of linoleate M + 18 spectra from brain stroke sample sprayed with and without 13C-labelled yeast extract. **e**, Comparison of linoleate M + 18 distribution on brain stroke samples sprayed with 13C-labelled yeast extract using different normalization methods. **f**, Comparison of linoleate M + 18 relative intensity in clusters 16 and its contralateral region using different normalization methods (n = 5 per group). 2-tailed Student's *t*-test was performed. All graph data are presented as mean values +/- SD. All scale bars, 600 µm.

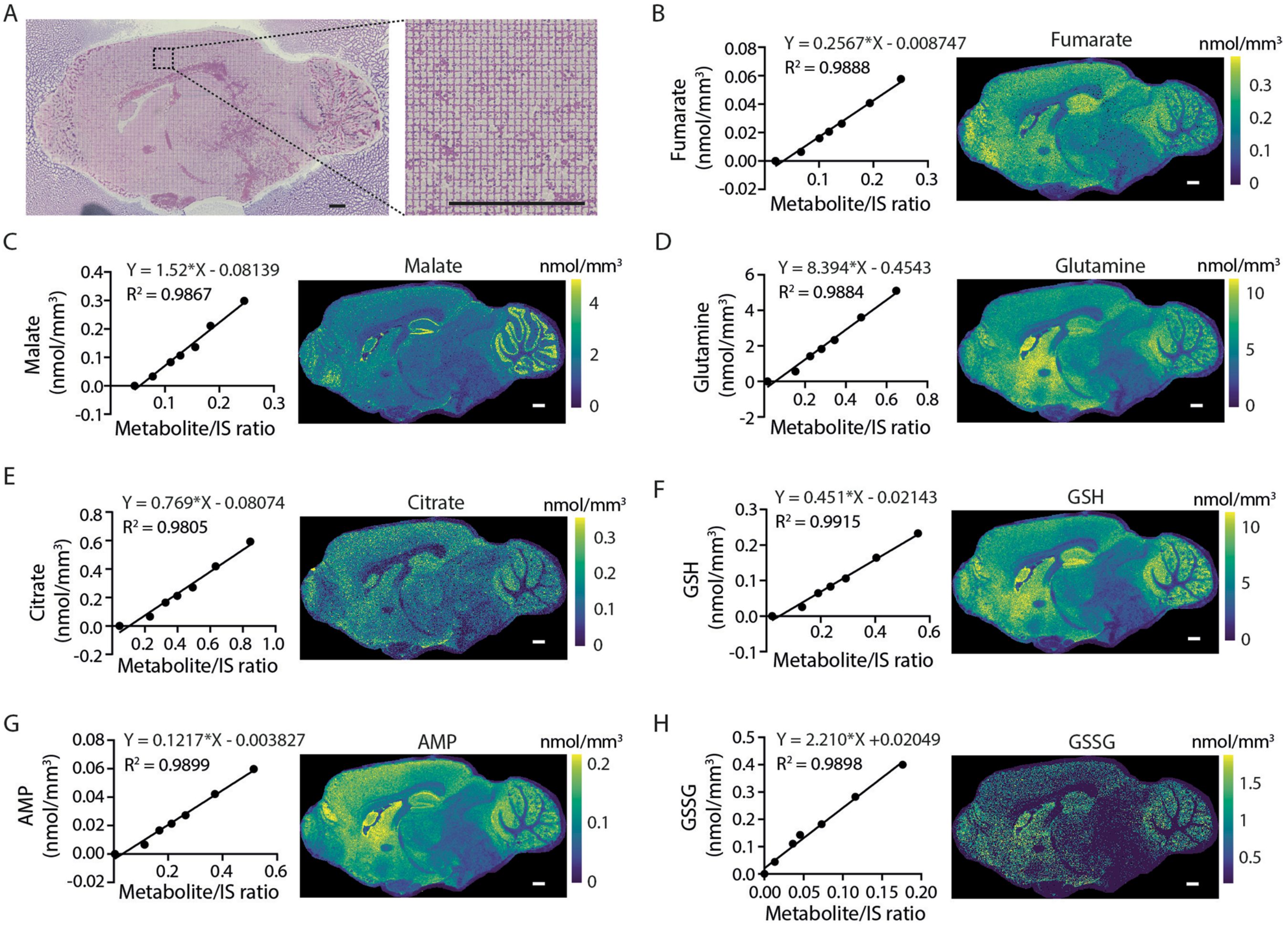

Extended Data Fig. 5 | Absolute spatial quantification of metabolites on mouse brain. a, Representative H&E staining of post-MSI tissue (n = 3). **b-h**, Calibration lines and absolute spatial quantification of fumarate **b**, malate **c**, glutamine **d**, citrate **e**, GSH **f**, AMP **g** and GSSG **h** on mouse brain.

nature portfolio

Corresponding author(s): Gangqi Wang
Last updated by author(s): Jun 9, 2025

Reporting Summary

Nature Portfolio wishes to improve the reproducibility of the work that we publish. This form provides structure for consistency and transparency in reporting. For further information on Nature Portfolio policies, see our Editorial Policies and the Editorial Policy Checklist.

Statistics

For all statistical analyses, confirm that the following items are present in the figure legend, table legend, main text, or Methods section.

n/a	Confirmed	
☐	☒	The exact sample size (*n*) for each experimental group/condition, given as a discrete number and unit of measurement
☐	☒	A statement on whether measurements were taken from distinct samples or whether the same sample was measured repeatedly
☐	☒	The statistical test(s) used AND whether they are one- or two-sided *Only common tests should be described solely by name; describe more complex techniques in the Methods section.*
☐	☒	A description of all covariates tested
☐	☒	A description of any assumptions or corrections, such as tests of normality and adjustment for multiple comparisons
☐	☒	A full description of the statistical parameters including central tendency (e.g. means) or other basic estimates (e.g. regression coefficient) AND variation (e.g. standard deviation) or associated estimates of uncertainty (e.g. confidence intervals)
☐	☒	For null hypothesis testing, the test statistic (e.g. *F*, *t*, *r*) with confidence intervals, effect sizes, degrees of freedom and *P* value noted *Give P values as exact values whenever suitable.*
☐	☒	For Bayesian analysis, information on the choice of priors and Markov chain Monte Carlo settings
☐	☒	For hierarchical and complex designs, identification of the appropriate level for tests and full reporting of outcomes
☒	☐	Estimates of effect sizes (e.g. Cohen's *d*, Pearson's *r*), indicating how they were calculated

Our web collection on statistics for biologists contains articles on many of the points above.

Software and code

Policy information about availability of computer code

Data collection	flexControl (Version 4.0, Bruker Daltonics);
Data analysis	SCiLS Lab 2023c Pro (SCiLS, Bruker Daltonics); Chenomx NMR suite 10.0 software (Chenomx NMR suite, v10.0, Edmonton, AB, Canada); Matlab R2019a; R (version 4.2); Seurat 4.3; GraphPad Prism 9; There is no new code generated specifically to this study. The codes used in this article is similar as in Github (https://github.com/Gangqiwang/scDYMO).

For manuscripts utilizing custom algorithms or software that are central to the research but not yet described in published literature, software must be made available to editors and reviewers. We strongly encourage code deposition in a community repository (e.g. GitHub). See the Nature Portfolio guidelines for submitting code & software for further information.

Data

Policy information about availability of data

All manuscripts must include a data availability statement. This statement should provide the following information, where applicable:

- Accession codes, unique identifiers, or web links for publicly available datasets
- A description of any restrictions on data availability
- For clinical datasets or third party data, please ensure that the statement adheres to our policy

The yeast metabolome database (https://www.ymdb.ca/), human metabolome database (https://hmdb.ca/) and LIPID MAPS (https://www.lipidmaps.org/) were used in this study. The total raw data size of this study is around 1TB. Due to the large size of all raw data, the exported and processed MSI data and parts of the raw

MSI data will bewere deposited in FigShare (https://doi.org/10.6084/m9.figshare.28665017.v1)upon publication, to provide the necessary information spectrum quality. For full availability of raw MALDI-MSI data related to this study, please contact Gangqi Wang (g.wang@lumc.nl) or Martin Giera (m.a.giera@lumc.nl) upon reasonable request data will be made available. Due to the large size of all raw data, the exported and processed MSI data and parts of the raw MSI data will bewere deposited in FigShare (https://doi.org/10.6084/m9.figshare.28665017.v1)upon publication, to provide the necessary information spectrum quality. For full availability of raw MALDI-MSI data related to this study, please contact Gangqi Wang (g.wang@lumc.nl) or Martin Giera (m.a.giera@lumc.nl) upon reasonable request data will be made available. Source data were provided with this article upon publication.

Human research participants

Policy information about studies involving human research participants and Sex and Gender in Research.

Reporting on sex and gender	NA
Population characteristics	NA
Recruitment	NA
Ethics oversight	NA

Note that full information on the approval of the study protocol must also be provided in the manuscript.

Field-specific reporting

Please select the one below that is the best fit for your research. If you are not sure, read the appropriate sections before making your selection.

☒ Life sciences ☐ Behavioural & social sciences ☐ Ecological, evolutionary & environmental sciences

For a reference copy of the document with all sections, see nature.com/documents/nr-reporting-summary-flat.pdf

Life sciences study design

All studies must disclose on these points even when the disclosure is negative.

Sample size	Mouse kidneys were obtained from normal 12-week-old male DBA/2J mice (n=3). Control mouse brains were obtained from normal 12-week-old male C57BL/6J mice (n=3). For brain stroke experiments, wild-type male C57BL6/J mice (aged 12-13 weeks) were used for the experiments (n=5 per group). No statistical methods were used to predetermine sample sizes, but our sample sizes are similar to those reported in previous publications.
Data exclusions	No data was excluded from the analyses.
Replication	All the experiments and data analysis were performed on 3 or 5 biological replicates (3 or 5 animals per group). All attempts at replication were successful.
Randomization	For brain stroke experiments, 10 mice were divided into 2 groups randomly (n = 5/group). For normal mouse kidneys and brains, 3 mice were selected randomly.
Blinding	This is not relevant in this study, since there was no group allocation.

Reporting for specific materials, systems and methods

We require information from authors about some types of materials, experimental systems and methods used in many studies. Here, indicate whether each material, system or method listed is relevant to your study. If you are not sure if a list item applies to your research, read the appropriate section before selecting a response.

Materials & experimental systems

n/a	Involved in the study	
☐	☒	Antibodies
☒	☐	Eukaryotic cell lines
☒	☐	Palaeontology and archaeology
☐	☒	Animals and other organisms
☒	☐	Clinical data
☒	☐	Dual use research of concern

Methods

n/a	Involved in the study	
☒	☐	ChIP-seq
☒	☐	Flow cytometry
☒	☐	MRI-based neuroimaging

Antibodies

Antibodies used	Anti-Myelin Basic Protein Antibody, a.a. 82-87 (1:200, MAB386, Sigma); Alexa Fluor 488 goat anti-rat (A11006, Invitrogen)
Validation	Anti-Myelin Basic Protein Antibody, a.a. 82-87 (1:200, MAB386, Sigma), biological source: Rat. clone name: 12. monoclonal; species reactivity: human, rat, sheep, mouse, rabbit, chicken, guinea pig, bovine, all; technique(s): ELISA: suitable, immunocytochemistry: suitable, immunohistochemistry: suitable, radioimmunoassay: suitable, western blot: suitable. isotype: IgG2a. Validation statements, relevant citation and other information can be found from the manufacturer's website: https://www.sigmaaldrich.com/NL/en/product/mm/mab386?srsltid=AfmBOopKxe3W8X5DSrkWuSkX46hcARu1OLOkaXxEmK0CT6Ji3svY4YqM Alexa Fluor 488 goat anti-rat (A11006, Invitrogen): https://www.thermofisher.com/antibody/product/Goat-anti-Rat-IgG-H-L-Cross-Adsorbed-Secondary-Antibody-Polyclonal/A-11006

Animals and other research organisms

Policy information about studies involving animals; ARRIVE guidelines recommended for reporting animal research, and Sex and Gender in Research

Laboratory animals	Mouse kidneys were obtained from normal 12-week-old male DBA/2J mice. Control mouse brains were obtained from normal 12-week-old male C57BL/6J mice. For brain stroke experiments, wild-type male C57BL6/J mice (aged 12-13 weeks) were used for the experiments.
Wild animals	the study did not involve wild animals
Reporting on sex	All the animal experiments were performed on male mice.
Field-collected samples	the study did not involve wild animals
Ethics oversight	Mouse kidneys were obtained from normal 12-week-old male DBA/2J mice (n=3). Animal experiments were approved by the Ethical Committee on Animal Care and Experimentation at the Leiden University Medical Center (Permit No. AVD1160020172926). Control mouse brains were obtained from normal 12-week-old male C57BL/6J mice (n=3). Animal experiments were approved by the Ethical Committee on Animal Care and Experimentation at the Leiden University Medical Center (Permit No. AVD11600202316801). For Brain stroke experiments, all animal procedures were performed in accordance with the guidelines for the use of experimental animals and were approved by the respective governmental committees (Regierungspraessidium Oberbayern, the Rhineland Palatinate Landesuntersuchungsamt Koblenz).

Note that full information on the approval of the study protocol must also be provided in the manuscript.